Impact of aerosols and clouds on decadal trends in all-sky solar radiation over the Netherlands (1966 – 2015)

Reinout Boers[1], Theo Brandsma[1] and A. Pier Siebesma[1]

[1]KNMI, De Bilt, PO Box 201, Netherlands

Correspondence to: Reinout Boers (reinout.boers@knmi.nl)

9   **Abstract.** A 50-year hourly dataset of global shortwave radiation, cloudiness and visibility over the Netherlands

10   was used to quantify the contribution of aerosols and clouds to the trend in yearly-averaged all-sky radiation

11   (1.81 ± 1.07 Wm^{-2}/decade). Yearly averaged clear-sky and cloud-base radiation data show large year-to-year

12   fluctuations caused by yearly changes in the occurrence of clear and cloudy periods and cannot be used for trend

13   analysis. Therefore, proxy clear-sky and cloud-base radiations were computed. In a proxy analysis hourly

14   radiation data falling within a fractional cloudiness value are fitted by monotonic increasing functions of solar

15   zenith angle and summed over all zenith angles occurring in a single year to produce an average. Stable trends

16   can then be computed from the proxy radiation data A functional expression is derived whereby the trend in

17   (proxy) all-sky radiation is a linear combination of trends in fractional cloudiness, (proxy) clear-sky radiation

18   and (proxy) cloud-base radiation. Trends (per decade) in fractional cloudiness, (proxy) clear-sky and (proxy)

19   cloud-base radiation were respectively 0.0097 ± 0.0062, 2.78 ± 0.50 Wm^{-2}, and 3.43 ± 1.17 Wm^{-2}. To add up to the

20   all-sky radiation the three trends have weight factors, namely the difference between the mean cloud-base and

21   clear-sky radiation, the clear-sky factor (1-fractional cloudiness) and the fractional cloudiness, respectively. Our

22   analysis clearly demonstrates that all three components contribute significantly to the observed trend in all-sky

23   radiation. Radiative transfer calculations using the aerosol optical thickness derived from visibility observations

24   indicate that Aerosol Radiation Interaction (ARI) is a strong candidate to explain the upward trend in the clear-

25   sky radiation. Aerosol Cloud Interaction (ACI) may have some impact on cloud-base radiation, but it is

26   suggested that decadal changes in cloud thickness and synoptic scale changes in cloud amount also play an

27   important role.

28   **1 Introduction**

29   Aerosols and clouds impact the solar radiation reaching the surface by radiative absorption and scattering.

30   Although there have been well-recorded trends in the all-sky radiation all over the globe it has been difficult to

31   precisely attribute such trends to trends in either aerosols or clouds. Wide-spread reductions in all-sky radiation

32   in the 1950 – 1970's ('dimming') have been followed by increases in later decades ('brightening'), especially in

33   Europe (Wild et al., 2005; Wild, 2009). Indeed, a thorough evaluation of all-sky radiation data over Europe

34   (Sanchez-Lorenzo et al., 2015) shows conclusively the distinct dip during the 1970's flanked on either side by

35   an earlier downward trend and a later upward trend. The later upward trends are thought to be the result of

36   changes in aerosol content and/or to changes in fractional cloudiness.

38   One issue hampering the understanding of records of all-sky radiation is that the impacts of aerosols and clouds

39   need to be derived from a single record at observational sites where additional data for instance from clouds,

40   were often not present. This has led some investigators to group data into regions and rely either on cloud data

41   from stations in the immediate surroundings or from satellites (or both) to supplement their radiation records

42   (Norris and Wild, 2007). Even though good results on trends in clear-sky radiation can be obtained at sites

43   where direct and solar radiation are recorded at the same time such as Baseline Surface Radiation Network

44   stations (Long and Ackermann, 2000; Long et al., 2009; Wild et al., 2005; Gan et al., 2009), most often an

45   investigator will have to rely on single global radiation data records that are specific to the region of interest

46   (such as Manara et. al., 2016) or on data stored in the Global Energy Balance Archive (GEBA) archive. GEBA

47   data can be used to good effect because of the fact that many stations have submitted data, but the peculiarities

48 of the radiative signals typical to individual localities are invariably lost in the abundance of data. It is therefore

49 of great importance that regional studies are carried out that record the changes in surface radiation in relation to

50 atmospheric parameters that can influence such changes.

51

52 In the context of Europe there have been a considerable number of regional studies that focus on trends in global

53 radiation and their attribution, such as in Germany (Liepert and Tegen, 2002; Liepert and Kukla, 1997; Liepert,

54 1997; Liepert, 2002)), in Germany and Switzerland combined (Ruckstuhl et al., 2008; Ruckstuhl and Norris,

55 2009; Ruckstuhl et al., 2010), in Estonia (Russak, 2009), in the general Baltic states (Ohvril et al., 2009), in

56 Spain (Mateos et al., 2014), in Norway (Parding et al., 2014), northern Europe in general (Stjern et al, 2009)

57 and in Italy (Manara et al., 2015). Even though there are regional differences the summarized global or all-sky

58 radiation data from Europe combined (Sanchez-Lorenzo et al, 2015) displays a minimum in 1984 – 1985 at the

59 end of a 'dimming' period with a subsequent return to higher values. The consensus about the decadal trends in

60 global radiation hides a considerable discourse about the attribution of the radiation trends. Of the parameters of

61 interest when investigating the trends in all-sky radiation namely clear-sky radiation, cloudy-sky radiation and

62 fractional cloudiness, the first two have been difficult to isolate from data and were addressed in only a few

63 studies (Wild, 2010). Yet an increasing number of studies indicate that there are good reasons to believe that

64 Aerosol Radiation Interaction (ARI) is responsible for the rise in all-sky radiation after 1985 (f.e. Philipona et al,

65 2009; Manara et al, 2016; Ruckstuhl et al, 2008) although the timing of the minimum or intensity cannot be

66 simulated very well using current aerosol emission inventories (Ruckstuhl and Norris, 2009; Liepert and Tegen,

67 2002, Romanou et al, 2007; Turnstock et al, 2015). About the influence of clouds, the situation continues to be

68 elusive. While it is obvious that clouds are important, the difficulty here is that there are several factors that

69 control their impact. For example there are considerable regional differences in fractional cloudiness (Norris,

70 2005): fractional cloudiness is constant in Northern Europe (Parding et al, 2014), in Germany before 1997

71 (Liepert, 1997) well after the minimum in global radiation in 1984, and is declining in the period after 1997 in

72 Switzerland and Germany, at least up to 2010 (Ruckstuhl et al, 2010). Furthermore, cloud optical thickness

73 changes can be the result of changes in microphysics or cloud thickness and current observations are not able to

74 separate the two effects. Nevertheless, modelling and observation studies by Romanou et al (2007), Ruckstuhl

75 and Norris (2009), Chiacchio and Wild (2010), Liepert (1997), Liepert and Kukla (1997), Long et al. (2009 and

76 Augustine and Dutton (2009)   suggest a definite but mixed role for clouds impacting the trend in all-sky

77 radiation.

78

79 Attribution studies using only surface-based observations must rely on supplemental data, namely those of

80 clouds (predominantly fractional cloudiness) and aerosols. Also, data on fractional cloudiness need to be

81 collected simultaneously with radiation data. Up to the mid-1990 clouds were observed by human observers but

82 since then the role of the observers is taken over by ceilometers. Apart from occasional sun photometer records

83 (Ruckstuhl et al (2008) data on aerosol are often unavailable. However, recent studies by Wu et al. (2014) and

84 Boers et al. (2015) have shown that it is possible to retrieve useful aerosol optical thickness data from surface

85 visibility records. The principal idea behind both studies is almost 50 years old (Eltermann, 1970; Kriebel, 1978;

86 Peterson and Fee, 1981; and revived by the work of Wang, 2009) and asserts that clear-sky optical thickness is

87 most often caused by aerosols residing in the planetary boundary layer which can be characterized by the optical

88 extinction at 550 nm. This parameter is by definition proportional to the inverse of atmospheric horizontal
89 visibility which in turn is a quantity abundantly observed over at least 50 years, often together with observations
90 of radiation.

91

92 Because of the importance attached to potential attribution of observed regional trends in all-sky radiation to
93 aerosols and / or clouds, we analyze hourly records of radiation, cloudiness and visibility data at five climate
94 stations in the Netherlands for the 50-year period 1966–2015. The two aims of this study are a) to quantify the
95 decomposition of the all-sky flux into its contributing components and compute the decadal trends in the
96 components, and b) to discern the relative importance of aerosols and clouds in shaping the observed trends.

97

98 The remainder of this paper is organized as follows: Section 2 describes briefly the theory and analysis
99 procedures to obtain clear and cloudy-sky signals from the all-sky data. The procedures combine radiation and
100 cloud coverage data. Equations are given describing the manner in which the all-sky radiation is explicitly
101 dependent upon fractional cloudiness, clear-sky radiation and radiation emanating at cloud-base. The equations
102 are based on elementary principles but we believe that this is the first time that these dependencies are explicitly
103 quantified, although the work by Liepert (1997), Liepert (2002), Liepert and Kukla (2002), and Ruckstuhl et al.
104 (2010) contain elements similar to our work. A full derivation of the equations is presented in the Appendix.

105

106 In section 3 the data analysis is discussed: all meta-data for all stations recorded between the late 1950's and
107 today were examined in order to better understand the impact of any changes in instruments and location and
108 calibrations on the data. Homogeneity tests were performed to discern any possible discontinuities in the data
109 and to understand whether all climate stations indeed belonged to the same climatological regime. Also attention
110 is given to a break in the cloud observations that occurred in 2002 with the transition from the human observer
111 to the ceilometer. Section 4 show the results. The relative influence of clear-sky radiation, cloudy-sky radiation
112 and fractional cloudiness on the all-sky radiation are shown. Also the relative merits of Aerosol Radiation
113 Interaction (ARI) and Aerosol Cloud Interaction (ACI) in influencing the all-sky radiation are discussed.

114

115 Section 5 concludes this paper with discussion and conclusions.

116 **2 Method**

117 **2.1 Radiation data, their proxies and trends**

118 An important aspect of this paper is to quantify the various radiative contributions to the all-sky radiation. It is
119 shown in this subsection that there is an elegant way to do so while invoking a minimum set of assumptions.
120 The radiative contributions arise from skies under clear, partly cloudy or overcast sky conditions. The presence
121 of cloud cover which is recorded simultaneously with the radiation assures that it is possible to quantify these
122 different contributions. Cloud cover is normally recorded in oktas (0-8) so that nine different contributions to the
123 radiation can be identified, which together build up the all-sky radiation.

124

125 For each okta value it will be assumed that the observed radiation is a linear combination of clear-sky radiation
126 and radiation emanating from cloud-base, each with cloud fraction weight factors that correspond to the okta

127 value at hand. The result is an equation which casts the all-sky radiation as a function of only three components:

128 1) the clear-sky radiation, 2) the cloud-base radiation and 3) the fractional cloudiness. Long term changes in

129 cloud type could perhaps affect cloud optical properties (liquid water versus ice water) but their influence on

130 trends is unknown and not studied here. The process to calculate the three components is then repeated for each

131 year in the period 1966 – 2015, resulting in three time series. The method thus assures that the relative

132 importance of clear-sky radiation, cloud-base radiation and fractional cloudiness to the trend in all-sky radiation

133 can be quantified.

134

135 Unfortunately, as has been shown before (Ruckstuhl et al., 2010) the analysis of trends using real data time

136 series is prone to large errors as periods of cloud and clear sky occur at random times throughout the year. Thus,

137 the year-to-year variations in averages are mostly the result in differences in the selection of solar zenith angles

138 used in constructing yearly averages. In the study of decadal variability that may be attributable to physical

139 causes this is an undesirable side effect so that an alternative method needs to be applied in the trend analysis.

140

141 The method we applied is coined an analysis of 'proxies'. We make use of the fact that for each okta value the

142 observed radiation data can be fitted by a monotonically increasing function of solar zenith angle. The line fit is

143 next evaluated at all hourly solar zenith angles occurring in a single year and averaged. The average proxy

144 radiation data that are thus obtained give a much more stable set of values from which (decadal) trends can be

145 calculated.

146

147 If S_k is the yearly averaged all-sky radiation (an observable), then S_{pk} is the yearly averaged all-sky proxy

148 radiation in year y_k. It can be shown that

149

150 $$S_{pk} = S_{p,c_0 k}(1 - c_k) + c_k S_{p,cloud,k} \qquad (1)$$

151 where $S_{p,c_0,k}$ is the yearly averaged clear-sky proxy radiation, c_k is the yearly averaged fractional cloudiness

152 and

153 $$S_{p,cloud,k} = \frac{\sum_{j=1}^{8} f_k(c_j) c_j S_{p,cb,c_j,k}}{\sum_{j=1}^{8} f_k(c_j) c_j} \qquad (2)$$

154 with $f_k(c_j)$ the fractional occurrence of okta j in a given year k, c_j the fractional cloudiness corresponding to

155 okta j, and $S_{p,cb,c_j,k}$ the cloud-base proxy radiation occurring at okta value j. A full derivation to arrive at Eq.

156 (1) is given in the Appendix.

157

158 In summary, The all-sky proxy radiation can be expressed as a linear combination of the clear-sky proxy, and

159 the cloud-base proxy radiation each weighted by their yearly mean coverage. Note that the real all-sky radiation

160 (S_k) and the proxy all-sky radiation (S_{pk}) are different, although they are of course quite close in value. S_k

161 is an observable, S_{pk} is derived from Eq. (1) after its components on the right side are first evaluated. However

162 an *a posteriori* comparison between the two has shown that they agree with each other better with a better than

163 5% margin.

164

165 Using Eq. (1) trends can be calculated using the deviation from the averages over the five decades:

166
$$S'_{pk} = c'_k(\overline{S_{p,cloud}} - \overline{S_{p,c_0}}) + (1-\bar{c})S'_{p,c_0,k} + \bar{c}S'_{p,cloud,k} + c'_k(S'_{cloud,k} - S'_{p,c_0,k}) \tag{3}$$

167 with

168 S'_{pk} is yearly deviation of the average over the five decades of the all-sky proxy radiation

169 c'_k is the yearly deviation of the average over the five decades of the fractional cloud cover

170 $\bar{c}$ is the average over the five decades of the fractional cloudiness

171 $S'_{p,c_0,k}$ is the yearly deviation of the average over the five decades of the clear-sky proxy radiation

172 $\overline{S_{p,c_0}}$ is the average over the five decades of the clear-sky proxy radiation

173 $S'_{p,cloud,k}$ is the yearly deviation of the average over the five decades of the cloud-base proxy radiation

174 $\overline{S_{p,cloud}}$ is the average over the five decades of the cloud-base proxy radiation.

175

176 The derivation of Eq. (3) is given in the Appendix.

177 Eq. (3) is the desired result for the analysis of trends. The first component on the right hand side represents

178 perturbations / trends in fractional cloudiness multiplied by the difference in cloud-base and clear-sky radiation,

179 which is negative. Therefore a positive trend in fractional cloudiness will impact as a negative trend component

180 in building up the all-sky radiation. The second term represents the clear-sky perturbations / trend weighted by

181 the average occurrence of clear skies (in our case approximately 0.32). The third term represents the

182 perturbations / trend in cloud-base radiation weighted by the fractional cloud cover (in our case approximately

183 0.68). The fourth term is a cross correlation term which in practice can be neglected.

184

185 Eq. (3) explains to a large extent the difficulties in attribution studies of the all-sky radiation. Not only the trends

186 in fractional cloudiness, clear-sky and cloud-base radiation are important, but also their relative weight as

187 determined by the mean fractional cloudiness and the difference between the mean clear-sky and cloud-base

188 radiation. In other words, there are a total of five different factors contributing to the trend in all-sky radiation.

189 For example, when the mean cloud fraction is large, as in northwestern Europe, the impact of the trend in clear-

190 sky radiation on the trend in all-sky radiation will be relatively modest in comparison to the impact of trend in

191 cloud-base radiation. The latter would be weighted by a factor 2 more than the trend in clear-sky radiation (0.32

192 versus 0.68).

193

194 Tests of trends will be performed using the standard Mann-Kendall (M-K) (Kendall, 1975) non-parametric test

195 often used in this type of analysis (see f.e. Long et al., 2009). after the time series was first decorrelated. The

196 uncertainty value attached to the trend is a test of significance indicating the 95% confidence interval of the

197 calculated slope line. The uncertainties in trend are due to two factors, namely those in yearly-averaged values
198 of S_p as a result of uncertainties in fitting constants in Eq. (A19) (see Appendix for details) and due to natural
199 variability of a multi-year or even decadal origin. Thus the stated uncertainty in output trend is a mix of both
200 factors.

201 **2.2 Retrieval of aerosol optical thickness**

202 Once the method to decompose the all-sky radiation into its clear-sky and cloudy-sky (proxy) components has
203 been applied and a trend analysis is performed, then it is our goal to seek an answer to the question which
204 processes might be responsible for their long-term change. Although possible long-term changes in the synoptic
205 conditions are a conceivable influence an obvious candidate for exploration of cause is the changing aerosol
206 content of the atmosphere. Aerosol content / concentration was not directly observed but visibility was recorded
207 throughout the period from which aerosol optical thickness was derived.
208

209 Aerosol optical thickness is the single most controlling factor in changing clear-sky radiation. A radiative
210 transfer model is used here to calculate the clear-sky radiation as a function of the changing optical thickness.
211 The output was compared to the observed clear-sky radiation. The process whereby aerosol can directly affect
212 clear-sky radiation is denoted as the aerosol direct effect or, using a term used in the IPCC (IPCC, 2013) report,
213 the Aerosol Radiation Interaction (ARI).
214

215 Aerosols can also affect the microphysical structure of clouds which in turn affects its radiative structure, a
216 process which is commonly denoted as the aerosol indirect effect, or Aerosol Cloud Interaction (ACI, as using
217 the terminology of IPCC, 2013).
218

219 The aerosol optical thickness of the atmosphere (τ_a) is a function of aerosol extinction (σ_a) integrated over the
220 depth of the atmosphere

221 $$\tau_a = \int_0^h \sigma_a dr = \int_0^h \int_r Qn(r)r^2 dr dz \qquad (4)$$

222

223 where Q is the scattering efficiency and can be obtained from Mie-calculations. The parameter n(r) is the
224 density of the size distribution and r is the radius of the particle. The vertical integration over height z is over the
225 depth of the atmosphere (h) and this yields using the Mean Value Theorem:

226 $$\tau_a \sim \sigma_{a,mean} H = Q_{mean} N_a H R^2 \qquad (5)$$

227

228 Here N_a is the concentration of aerosols, R is the mean size of the aerosol particles and H is a scaling depth
229 proportional to the depth of the planetary boundary layer. The proportionality factor includes all vertical
230 variations in aerosol, size distribution and optical properties. Aerosol extinction can be approximated as
231 (Eltermann, 1970; Kriebel, 1978, Peterson and Fee, 1981; Wang et al., 2009)

232 $$\sigma_{a,mean} = \frac{-\log_e (0.05)}{Visibility} \qquad (6)$$

234 Visibility is a measurable quantity and it provides a means to compute aerosol optical thickness at hourly

235 intervals from standard weather station observations. This procedure has been used to obtain decadal time series

236 of the aerosol optical thickness over the Netherlands and China (Boers et al, 2015; Wu et al., 2014). We

237 examined the European Center for Medium Range Weather Forecast Reanalysis (ERA) data (Dee et al., 2011)

238 for changes in the planetary boundary layer depth. No indications for changes were found in the course of 50

239 years and a value of 1000 m was used to reflect conditions over the Netherlands.

2.3 Radiative transfer calculations

241 Variations or trends in solar radiation under cloudless conditions are mostly caused by variations in the optical

242 properties and concentrations of aerosols, the ARI. The principle aim here is to assess whether the variations in

243 optical properties can explain the observed variations in solar radiation. For this purpose, we used a simple

244 radiation transfer model based on the delta-Eddington two−stream approach, as added complexity in radiative

245 transfer models will not increase the confidence in our results (Boers et al., 1994).

247 For model calculations, the parameters affecting the radiation are aerosol optical thickness, single scattering

248 albedo, asymmetry parameter and Ångstrøm parameter. Of these four parameters the first two are the most

249 important and only the first one can be obtained from observations. It was attempted to derive the single

250 scattering albedo and its time variation from the aerosol composition in the Netherlands (Boers et al., 2015) but

251 its precise quantification remains elusive due to its uncertain dependence on aerosol composition, wavelength,

252 aerosol hygroscopicity and relative humidity. Thus a constant value of 0.90 was used instead. The results of

253 Boers et al. (2015) indicate that a considerable portion of the reduction in aerosol optical thickness or potential

254 solar brightening can be attributed to the reduction of sulphate aerosols after the 1980's. Even though the nitrate

255 values did increase over the same time, their increases cannot completely counterbalance the decreasing

256 sulphate concentrations. The asymmetry parameter and the Ångstrøm parameter are set to 0.69 and 1.5

257 respectively to reflect typical aerosol values derived for the Netherlands (Boers et al., 2015).

2.4 Solar radiation and aerosol-cloud interaction

259 Variations or trends in solar radiation emanating from the action of clouds are mostly caused by variations in the

260 cloud fractional coverage and by variations in the optical properties and concentrations of droplets or ice. The

261 two main hypotheses for ACI to operate on cloud properties are formulated below as Hypothesis 1 and 2, in the

262 remainder of this paper referred to as ACI-I, and ACI-II, respectively. ACI-I suggests that variations in cloud

263 optical properties are attributable to variations in aerosol concentration itself. A massive amount of literature has

264 been devoted to this subject, but Twomey (1977) is the first one to describe this effect. It is based on a causal

265 link between changes in aerosol concentration (N_a) and cloud droplet concentration (N_c). These two parameters

266 are not necessarily linearly linked: as the amount of aerosol particles increases, it becomes more and more

267 difficult to raise the supersaturation necessary to activate additional particles. Therefore, N_c and N_a are often

268 related by means of a logarithmic function or a power law with exponent smaller than one (Jones et al., 1994;

269 Gultepe and Isaac, 1995), e.g..

270 $$N_c \sim N_a^{0.26} \tag{7}$$

271 Only a limited amount of aerosol particles will be activated to cloud droplets and incipient water droplets all

272 compete for the same amount of water vapor as they grow. This means that the mean size of cloud droplets

273 decreases as the number of cloud droplets increases. The consequence for the cloud optical thickness (Twomey,

274 1977) is that :

275 $\qquad \tau_{c,ACI} \sim H_c N_c^{1/3}$ (8)

276

277 Here H_c is the depth of the cloud and $\tau_{c,ACI}$ is the cloud optical thickness attributable to the aerosol aerosol-cloud

278 interaction (ACI-I). Thus, compared to Eq.(5) where the equivalent link between aerosol optical thickness and

279 aerosol number concentration is described the dependence of cloud optical depth to number concentration is

280 much weaker.

281

282 Combining Eqs. (7) and (8) with Eq. (5) we find:

283 $\qquad \tau_{c,ACI} \sim \tau_a^{0.26/3}$ (9)

284

285 As the cloud optical thickness τ_c (which is due to the ACI –I and other causes) can be obtained from inverting

286 the cloud-base radiative fluxes and τ_a can be obtained from Eqs (7), (8), the validity of the Eq. (9) can be

287 studied.

288

289 ACI-II suggests that increasing N_c will result in suppression of precipitation so that cloud life time and cloud

290 fraction is increased (Albrecht, 1989). In our analysis, cloud fraction is obtained in a straightforward manner by

291 counting the hourly cloud data so that the hypothesis that changes in aerosol results in changes in cloud cover

292 can be tested.

293 **3 Data analysis**

294 **3.1 Data sources**

295 We used quality controlled time series of hourly data of surface radiation, cloudiness and visibility which are

296 standard output commonly available to the general public and submitted to the traditional climate data

297 repositories. The surface radiation data consist of 10 second data for shortwave radiation instruments integrated

298 over the hour. To be consistent with most publications on the subject of trends in radiation, the hourly average is

299 taken and expressed in Wm^{-2}. The visibility is recorded at the end of each hour, either by the Human Observer

300 (until 2002) or taken from a Present Weather Sensor (PWS, after 2002). The PWS detects the forward scattering

301 of light emitted by a Near Infrared Light Emitting Diode under an angle of 42°. Cloud cover is observed by the

302 Human Observer until 2002 and represents the last 10 minutes of every hour. After 2002 it is observed by a

303 vertically pointing ceilometer and represents the average of the last 30 minutes of the hour.

304

305 A serious concern is that conditional sampling was done on the radiation data in a situation where the

306 observation that represents the condition (namely whether or not clouds are present), was not taken in exactly

307 the same time interval as the observation (radiation) itself. Therefore the conditionally sampled data are an

308 imperfect representation of the true situation. This is particularly true for rapidly changing cloudiness
309 conditions. This issue cannot be rectified. However, in this paper exclusive use is made of yearly averages of
310 conditionally sampled radiation data. For these data, the averaging procedure cancels out data with too much or
311 too few clouds within the hour of the selected radiation data, so that the variability observed in the data will be
312 simply enhanced random noise.

313 **3.2 Metadata**

314 Table 1 presents the basic metadata of the five principal climate stations in the Netherlands together with the
315 dates when the collection of radiation data started. The station metadata archive was analyzed from which it was
316 apparent that initially the regular maintenance and understanding of instruments was inadequate. Typical
317 problems that needed to be overcome were the build-up of moisture between the concentric glass half-domes,
318 the removal of dust and bird droppings, the horizontal alignment of the instrument and the proper positioning of
319 instruments with respect to shading obstacles such as (growing) trees.
320
321 Apart from these issues, insufficient (re)calibration of the instruments, irregular replacement / rotation of
322 instruments from the instrument pool are the reason that the initial years of observation often yielded data of
323 dubious quality. In the end it was decided to discard all data from the climate stations before the year 1966. The
324 data from the station De Bilt are of acceptable quality from 1961 onwards, in particular since from that year
325 onward radiation was measured by two radiometers that were placed side-by-side. However these earlier data
326 will not be used here because this would induce unacceptable weighting on this station of the radiation average
327 in the five year period prior to the year 1966.

328 **3.3 Homogeneity test**

329 Even though some investigators have attempted with some success to homogenize and gap-fill their data
330 (Manara et al, 2016) for a small region of the Netherlands with few stations (in our case 5) such a
331 homogenization procedure is unlikely to be successful. The reason is that it carries the risk of replacing real data
332 with bogus data which would weigh heavily on the few data time series available. Nevertheless it is instructive
333 to apply a homogeneity test to understand differences between the time series.
334
335 The five radiation time series were analyzed for statistical homogeneity using the Standard Normal
336 Homogeneity Test (SNHT; Alexanderson, 1986). Instead of applying SNHT directly to each station series, we
337 used relative testing. Relative testing removes the natural variation from a time series (while assuming that
338 natural variation is about the same for all locations), which increases the probability of detecting statistically
339 significant breaks. The SNHT was twice applied to each station series. In the first test each station series was
340 subtracted by the mean of the four other station time series. In the second test each station series was subtracted
341 by the other four station time series separately. The latter would reveal a break in the series. Note however that
342 the results yield potential statistical breaks, not real ones.
343
344 The homogeneity testing was applied to the 1966-2015 period. The results indicate that De Bilt data are
345 different from the others in the 1966-1975 period, though a possible inhomogeneity reveals itself only in two of

the four relative series. From the metadata there is, however, no reason to doubt the quality of the series of De Bilt in this particular period. In fact of all five stations the instruments at the De Bilt observatory were probably maintained in the most optimum way. Also, the series of Eelde appears to be high relative to the other four station for the 1966 -1972 period although again from the metadata there is no reason to judge the series of Eelde in this particular period as suspect. Eelde is the most north-easterly station in the Netherlands and data from this station were compared to the most nearby German station with a long radiation time series (Norderney, 1967 – 2015). This comparison indicated that Eelde is homogeneous with Norderney, strongly suggesting that the relative high values of radiation at Eelde in the period 1966 – 1972 are indicative of real atmospheric variability rather than instrumental problems.

A similar homogeneity test was applied to the standard aerosol optical thickness output from the stations based on Eq. (6) which in turn are based on the visibility observations. No discontinuity was detected at the year 2002 indicating good adjustment procedures from Human Observer to instrument at the transition time. From these tests it emerges that the stations Vlissingen and De Bilt depart the most from the average. Furthermore, when all stations are compared, De Bilt departs the most from the other four. Again these differences can very well imply real differences between station, such as for example may be the result of local differences in air pollution that influence visibility (and thus optical thickness).

For the remainder of the research we decided to use the mean of all five stations for the 1966-2015 period. We studied the sensitivity of the results to leaving out stations and found that even though some details were different, it did not significantly alter any of the findings and conclusions.

3.4 Okta and cloud amount

Even though cloud amount is commonly indicated with the parameter okta, its translation to actual cloud amount as a fraction is necessary for usage in this paper. According to World Meteorological Organization guidelines (WMO, 2008) actual cloud amount should be indicated as one okta in case a single cloud is present in an otherwise completely clear-sky. Similarly, if a single hole exist in an otherwise overcast sky cloud amount should be indicated as seven out of eight. Therefore, a cloud amount of one okta corresponds to a lower cloud amount than expected based on the numerical value of one-eighth. Similarly, a cloud amount of seven-eighth corresponds to a larger value than indicated by its numerical value. Boers et al. (2010) evaluated observed cloud amounts expressed in oktas with fractional cloud amounts derived from all-sky observation of clouds using a Total Sky Imager (an instrument sensitive to radiation in the visible part of the solar spectrum) and using a Nubiscope (an all-sky scanning infrared radiometer). We adhere to the results of their study (their section 2.3, table 1) where for okta 0-8 the following cloud amounts are given (in percentage): 0.00, 6.15, 24.94, 37.51, 50.03, 62.56, 75.18, 95.07, 100.

In the analysis presented in the next section a practical problem occurred in distinguishing between radiation emanating from a completely clear-sky or from a sky with a single cloud but otherwise clear. In the latter case, provided that the cloud does not completely block the direct solar beam, it will be impossible to discern whether the radiative flux would have come from a sky with the okta=0. For this reason it was decided to take data from

385 c=0 and c=1 together and designated the combined data as 'clear-sky'. A similar argument can be made for the

386 radiation at the high end of cloudiness. Hence, data from c=7 and c=8 were lumped together as designating an

387 'overcast' sky.

3.5 Discontinuity in 2002

389 During the year 2002 the Human Observer was replaced by the Present Weather Sensor for visibility

390 observations and by the ceilometer for cloud observations. While the former transition posed little problems in

391 the analysis of data, such was not the case for the latter. When observing clouds the Human Observer takes into

392 account the full 360-degree view of the horizon. A ceilometer only observes a narrow portion of the sky in

393 vertical direction. Although the half –hour averaging of the cloud observations to some extent compensates for

394 the absence of instantaneous hemispheric information, the two types of observation represent different methods

395 of estimating cloud cover so that the conditional sampling of the radiation is significantly affected. For example,

396 the digital nature of the ceilometer observation results in many more observations in the $c = 0$ (cloudless) and

397 the $c = 8$ (overcast) cloud cover selection bin than obtained from the Human Observer (Boers et al., 2010). As a

398 result, the selectively sampled radiation data in both okta bins will be contaminated by data recorded under

399 fractionally cloudy conditions. Contamination by other okta values is also present for data selected for each of

400 the $1 - 7$ okta range but less than for overcast sky conditions. As a result, the selectively sampled radiation data

401 showed distinct discontinuities in 2002.

402

403 To account for the discontinuity we decided to apply a so-called quantile-quantile correction to the frequency

404 distribution of cloud coverage from the period after 2002 (during which the ceilometer was operative) and adjust

405 it to the frequency distribution from the period before 2002 (during which the Human Observer was operative).

406 The quantile-quantile correction (Li et al., 2010) is commonly used to adjust distributions of meteorological

407 parameters of numerical models to observed distributions of the same parameters. As a first step cloud cover

408 data (converted from okta to fractional cloudiness, see section 3.4) from the period $2002 - 2015$ was smoothed

409 by a Gaussian filter with a half-width of two data points (i.e. two hours). This produced a smooth distribution

410 which, when converted back to okta, yielded a distribution similar but not the same to the okta distribution of

411 the Human Observer. The next step was to do a quantile-quantile correction on the smoothed data. The

412 credibility of a quantile-quantile correction depends on whether it can be assured that the average distribution

413 function as observed by the Human Observer does not change over the break (in case the Human Observer

414 would have made the observations after the break). Although there were some long-term changes in the

415 distribution function before the year 2002 they were small enough to assume the invariance of the distribution

416 function over the break. With the application of the quantile-quantile correction the okta values and hence the

417 fractional cloudiness values after the break assume new / corrected values that are applied as new / corrected

418 discriminators in the selection of the radiative flux.

419

420 As a proof of soundness of the procedure we applied the quantile – quantile correction and recomputed the

421 fractional cloudiness as the summation $\sum_{1}^{8} f_i c_i = \bar{c}$ (see discussion beneath Eq. (A4) in the Appendix) and

compared the result to satellite observations derived from successive NOAA-satellites (Karlsson et al, 2017). Figure 1 shows the results.

The NOAA data (red line) comprises an average over the Netherlands and have been bias-corrected. It is clear that the surface data (black line) which are break-corrected after the year 2002 provides an excellent agreement to the NOAA data when compared to the data which are not-break corrected (blue line). Note also that the data that are not break-corrected show a downward trend in cloudiness while the break-corrected data show an upward trend. These results are thus at odds with observations in Germany close to the Netherlands (Ruckstuhl et al, 2010) where cloud cover seems to be declining at least until 2010.

4 Results

4.1 Decomposing the all-sky radiative fluxes

As a first step in understanding the relative impact of clear and cloudy skies on the all-sky radiative flux it is instructive to examine the manner in which the top-of-atmosphere (TOA) radiative flux is reduced by the various constituents and scattering and absorption mechanisms in the atmosphere (Figure 2). The combined effect of all these processes is responsible for reducing the TOA radiative fluxes down to the observed all-sky radiative flux as indicated by the white line at the bottom of the figure. Figure 2 is a combination of calculations and observations. Observed are the all-sky flux (the white line at the bottom of the Figure) and the clear-sky flux (the white line in the middle). Starting from the top downward, the first reduction of the TOA flux is due to Rayleigh scattering, namely downwards from 274 to 253 Wm^{-2}. Continuing downwards ozone absorption is responsible for a further reduction from 253 to 246 Wm^{-2}. Next water vapor absorption reduces the radiative flux by a further 39 Wm^{-2} from 246 to 207 Wm^{-2}. These three decrements were calculated from inputs from the European Centre for Medium Range Weather Forecast's Re-Analysis project, ERA (for the ozone and water vapor absorption) or surface pressure observations (for the Rayleigh scattering).

The next reduction is due to the aerosol scattering and absorption which takes the radiative flux further down to the observed clear-sky flux (or more precisely the proxy) from 207 Wm^{-2} to ~170 Wm^{-2} around 1970 or to ~185 Wm^{-2} near 2015 with a steady increasing value during the intermediate years. The solid white line in the middle of the plot represents the clear-sky flux. The rest of the reduction from the clear-sky radiative flux to the all-sky flux is entirely due to the action of clouds. The observed clear-sky (proxy) shortwave radiation shows that about 13.6 $W\ m^{-2}$ has been added to the clear-sky radiation over a period of 5 decades. A trend value at 2.78±0.50 $W\ m^{-2}$ / decade was calculated. The upward trend in clear-sky radiation is thus deemed to be strongly significant. The lower white solid line represents the all-sky radiation which is derived straight from the publicly available climate data sources. It shows considerable short-term variations but overall there is a positive trend. The trend value was calculated as 1.81±1.07 $W\ m^{-2}$ / decade and is thus also considered significant.

When comparing the different contributions there are three important points to be considered. First, the combined effects of Rayleigh scattering, ozone and water vapor absorption is constant over time. Even though there is a slight increase in water vapor path over the 50-year period, this is not reflected in any discernable

decrease in radiative flux. Second, despite the absence of any significant trends in the respective radiative reductions they make up a very substantial part of the overall reduction from the TOA radiative flux to the all-sky flux (40 – 50%). Third, the two-pronged action of clouds by 1) blocking part of clear-sky flux in reaching the surface and 2) by scattering radiation inside the clouds is considerably larger than the action of scattering and absorption of radiation by aerosols in reducing the TOA radiative flux. The former ranging from double the latter at the beginning of the period to triple the latter at the end of the period.

Figure 3 shows the measured all-sky radiation and the proxy clear-sky and weighted cloud-base radiation. Linear regression lines (blue) as well as a 21-point Gaussian fit (red) are shown in the figure. There is a weak minimum in all-sky radiation at 1984 which is matched by a minimum in cloud-base radiation near 1982 – 1984. In contrast the clear-sky radiation has an upward trend throughout the entire period. All trend are significant when taken over the entire period.

Figure 4 shows the key result of this paper namely the reconstruction of the trend in the all-sky (proxy) flux out of its three main components as formulated in Eq. (3). Here, the last term, a cross correlation term is not shown on account of its very small yearly values (less than $0.5 \ \mathrm{W \ m^{-2}}$). The black curve shows the variation in all-sky proxy radiation as a function of time. Note again that this function is slightly different from the real all-sky radiation data as its construction is based on the proxy data. Even so, the fluctuations and trends in the proxy data are clearly very close to the fluctuations and trends as observed in the real all-sky data of Figure 3. However, the Gaussian-filtered data indicates that the weak minimum in the original data is replaced by a (close to) constant value in the proxy data. The red curve is the contribution to the trend in all-sky proxy radiation due to the trend in cloud amount. Cloud amount is increasing and as a consequence the contribution to the overall trend in solar radiation is negative. The green line is the contribution to the trend in all-sky proxy radiation as a result of the positive trend in clear-sky proxy radiation, but modulated by the average fraction of time that it is actually clear (32%). The blue line is the contribution to the trend in all-sky radiation as a result of the positive trend in proxy cloud-base radiation. It has a broad minimum, but modulated by the fraction that it is cloudy on average (68%). Each curve represents a perturbation with respect to its average and the large tick marks represent intervals of $10 \ \mathrm{W \ m^{-2}}$.

A number of intermediate conclusions can be drawn at this point:
1. The cloud-base and cloud cover contributing trends are of the same order of magnitude whereas the clear-sky trend contribution is less significant than either one of them.
2. As the mean fractional cloudiness at 0.68 is larger than 0.50, the contribution to the all-sky flux due to a trend in cloud-base radiation has a comparatively larger weight than the contribution of the trend in clear-sky radiation.
3. The increase in cloud cover results in a negative trend contribution to the trend in all-sky (proxy) radiation which thus dampens the strong trend contribution due to the increasing cloud-base proxy radiation. The implication is that clouds have become (optically thinner) but at the same time more frequent, the cause of which is unclear.

4. The short-term variations in all-sky radiation are almost entirely due to the short-term variations in fractional cloudiness.

5. The weak minimum (constant) in all-sky (proxy) radiation is strongly linked to trends in clouds, but not as much to the trend in clear-sky radiation.

Table 2 summarizes the results of the trend analysis. Here, also a subselection is made according to the time period over which trend analysis is performed. Significance is indicated in the last column. Note that both the trends in all-sky radiation and the trend in all-sky proxy radiation are given in the table. The trend in all-sky radiation is simply inferred from the data whereas the trend in all-sky proxy radiation is computed from Eq. (3). Thus, contrary to common notion the trend in measured all-sky radiation cannot be recovered from the trends in proxy data. It is only the all-sky proxy trend that can be recovered from the clear-sky proxy term and the cloud-base proxy term of Eq. (3) and in addition from the fractional cloudiness term of Eq. (3). Note furthermore that the fractional cloudiness term in Eq. (3) is a scaled version of the trend in fractional cloudiness, whereas the other two are scaled versions of the trend in clear-sky proxy radiation and cloud-base proxy radiation.

Inspection of the table indicates that none of the trends (including those of the clear-sky proxy radiation) is significant in the period 1966 – 1984. All significant trends occur in the period 1984 – 2015. Two-thirds of the strong upward trend in cloud-base proxy radiation is offset by cloud fraction trend term in the same period.

To our knowledge these calculations are the first of their kind and demonstrate the relative importance of the impacts of clear and cloudy skies on the all-sky radiation. Trend values for the all-sky radiation all fall within the bounds of Sanchez-Lorenzo et al. (2015) given by their comprehensive summary of Europe's observations. For the clear-sky proxy radiation the trend is positive throughout the entire period and the absence of a curvature matching that of the all-sky radiation does not suggest a very strong causal link with it. In contrast the curvature of the cloud-base proxy radiation curve much more resembles that of the all-sky radiation. Because the fractional cloud cover term partly compensates the strong upward trend of the cloud-base curve after 1985, it strongly suggests that for the Netherlands cloud processes are the dominant factor that impact the shape of the all-sky radiation time series.

4.2 Aerosol-radiation interaction (ARI)

To investigate the possibility of aerosol-radiation interaction the median aerosol optical thickness is derived from the visibility observations. Next radiative transfer model calculations were performed to compute the solar radiation. Figure 5 shows the time series of median aerosol optical thickness for the Netherlands. To about 1985 the optical thickness has a weakly downward trend albeit that there are considerable year-to-year variations. After 1985 there is a distinct downward trend that remains present until the end of the time series in 2015. Overall trend is -0.032 per decade and is significant.

Figure 6 shows the results from radiative transfer computation compared to the clear-sky flux. The solid black and accompanying shading represents the best fit through the data (the points connected by a black line). The blue line is the result of calculating the clear-sky radiation using the aerosol optical thickness in Figure 5 as an input, with a fixed value of the single scattering albedo of 0.90. The calculations indicate a remarkable

538 agreement with the observed clear-sky radiation. The blue line falls entirely within the shaded area of
539 uncertainty of the slope through the data.

540

541 The accuracy of the modeled radiation curves is dependent upon the accuracy of the optical thickness derived
542 from the visibility observations and the value of the single scattering albedo. If the scaling depth used to match
543 the optical thickness observations to satellite and surface-base radiation data (Boers et al., 2015) is changed, so
544 will the position of the model output (blue line) change with respect to the clear – air data ($\delta SW = 5 - 6\,W\,m^{-2}$
545 for $\delta\tau$ = -0.1).

546

547 There is however no useful information on the time-dependence of the single scattering albedo, the mean value
548 of which is not clear either. The value of 0.90 as used here reflects a compromise between the necessity of
549 having to assign it a value less than one due to the presence of radiation absorbing aerosols (Black Carbon and
550 Organic Aerosols), and the prevalence of pure scattering aerosols in an environment of high relative humidity
551 (sulfates and nitrates) which tend to keep the single scattering albedo at a high value.

552

553 However, the overall conclusion is that the reduction in aerosol concentration resulting in a reduction in aerosol
554 optical thickness is a very strong candidate cause explaining the overall increase in clear-sky solar radiation.
555 This implies that there is a compelling argument that ARI i.e. the direct aerosol effect is responsible for the
556 decadal change in clear-sky radiation.

557 **4.3 Aerosol-cloud interaction (ACI)**

558 Concerning ACI-I we plotted the left and right sides of the function described in Eq. (9). Here (Figure 7) the
559 cloud optical thickness for clouds has been derived from the monotonic relationship between solar radiation and
560 cloud optical thickness and using the mean weighted cloud-base radiation (bottom curve in Figure 2) as the
561 radiative input. The cloud optical thickness that is thus derived constitutes the left side of Eq. (9). The right side
562 of Eq. (9) is based on the aerosol optical thickness data as shown in Figure 5. According to Figure 7, there is
563 indeed an indication that there may be a link between the two optical thicknesses but the regression line has a
564 larger slope than suggested by Eq. (9). This suggests that there may be other mechanisms that play a role in
565 changing the cloud optical thickness. The most likely candidate responsible for these additional changes is a
566 decadal thinning of clouds. However, there is no confirmation by independent data sources suggesting that such
567 thinning has indeed taken place over the course of five decades.

568

569 Under ACI-II cloud amount is governed by precipitation. Here a reduction in aerosols over time would increase
570 the size of cloud droplets, thus enhancing the fall-out of liquid water and thus reducing cloud amount. However,
571 data shown in Figure 1 indicate that cloud fraction is increasing after 1985 when at the same time the aerosol
572 optical thickness decreases. This does not necessarily mean that ACI-II is not operative, but that other factors
573 (such as large scale synoptic changes) at least overwhelm any possible cloud cover changes due to ACI-II.

574

5 Discussion and conclusions

Our derivation of a trend equation for the all-sky radiation shows that there are five parameters that influence the trend, namely 1) a trend in fractional cloudiness, 2) a trend in clear-sky radiation, 3) a trend in cloud-base radiation, 4) the decadal mean of the fractional cloudiness, and 5) the difference between the decadal means of the cloud-base and the clear-sky radiation. It is therefore not surprising that it has been difficult up to now to come up with any firm conclusions about the relative importance of trends in clouds or clear-sky radiation in contributing to the trend in all-sky radiation. This situation is further hampered by difficulties in the derivation of clear-sky and cloud-base radiation, requiring a specialized analysis removing the year-to-year internal fluctuations in radiation estimates. They are the results of periodic synoptic conditions that favor certain cloudiness conditions. An analysis of annual means of radiation selected under specific okta values will produce unrealistic results, as noted by Ruckstuhl et al (2010). In order to overcome this last issue we have cast the problem of estimating annual mean radiation in a two-dimensional framework with cloud fraction (okta) and cosine of solar zenith angle as the two controlling variables. A proxy radiation is derived by fitting per okta value a function that is solely dependent upon cosine of zenith angle. Next annual means are computed using the annually constant distribution of cosine values. Stable values of radiation ensue from which trends can be calculated.

Our analysis comprises 50 years of hourly radiation, cloudiness and visibility data at the five principal climate stations in the Netherlands. We summarize the main conclusions of this work.

1) The three most important mechanisms reducing the top-of-the-atmosphere radiation to the observed all-sky radiation are absorption of radiation by water vapor, and scattering and absorption by aerosols and clouds. Over the Netherlands the reduction in radiation due to water vapor absorption is actually larger than from aerosol scattering and absorption. However, as there is no trend in water vapor, there is no trend in the all-sky radiation due to trends in water vapor.

2) Trends in clear-sky, cloud-base radiation and fractional cloudiness are all important in contributing to the trend in all-sky radiation.

3) Over the Netherlands the clear-sky trend is weighted by 0.32 which is one minus the decadal mean fractional cloud cover and the cloudy-sky trend is weighted by 0.68 (i.e. the decadal mean of fractional cloudiness). Therefore, in the Netherlands a trend in cloud-base radiation has double the weight of a clear-sky radiation trend in contributing to the all-sky radiation trend. Thus, in a general sense this means that the actual value of fractional cloudiness, which has a strong regional dependence, exerts a considerable control over the relative importance of clear-sky and cloud-base radiation trends.

4) Over the Netherlands the trend in fractional cloudiness is significantly positive in the period after 1985 and because this trend is multiplied by the (negative) difference between the decadal means of cloud-base and clear-sky radiation, it contributes as a negative trend to the trend in all-sky radiation. As the literature suggests (f.e. Norris, 2005) there are significant regional differences in long term trends in cloud cover, so it indicates that strong regional differences will exist in its contribution to the trend in all-sky radiation.

5) As found in most studies (see summary of Sanchez-Lorenzo et al., 2015), a minimum in all-sky radiation is found around 1985. The negative trend of -1.4 Wm^{-2} up to 1985 is weaker than the average

of Europe (-2.5 Wm^{-2}). The upward trend from 1985 onwards of 2.3 Wm^{-2} is also weaker than the average of Europe (3.2 Wm^{-2}).

6) The minimum in all-sky radiation is not matched by a corresponding minimum in clear-sky proxy radiation. An increasing trend of 1.22 Wm^{-2} is found over the earlier period which increased to 3.40 Wm^{-2} later on. After significant amounts of local natural gas were found in the late 1950s the Netherlands were a very early (1960 – 1965) adapter to cleaner fuels which may explain the increase in clear-sky radiation in the earlier period (1966-1985).

7) The trend in cloud-base radiation has a similar shape as that of the all-sky radiation. It is weakly negative before 1985 (-0.77 Wm^{-2}) and strongly positive thereafter (4.94 Wm^{-2}). Consequently, the conclusion is justified that the curvature /weak minimum in all-sky radiation around 1985 is caused mostly by the cloud-base radiation.

8) As our techniques are able to isolate the clear-sky radiative component it has been possible to study the attribution of changes in aerosol content to the observed trend in clear-sky radiation. Radiative transfer calculations demonstrate that the increase in clear-sky radiation can be completely explained by a concomitant decrease in aerosol optical thickness. This strongly suggests that the ARI (the direct aerosol effect) is a prime candidate to explain the observed increase in clear-sky radiation.

9) Similarly, ACI-I and ACI-II have been studied to understand their potential impact on the all-sky radiation. Neither is shown to have a dominant contribution to the trend in the overall all-sky flux but the potential influence of ACI-I and ACI-II cannot be ruled out by the data: There may be other influencing mechanisms that mask the impact of ACI-I and ACI-II such as decadal changes in cloud thickness and fractional cloudiness as a result of large-scale synoptic phenomena.

Prerequisite for our method to work is the availability of simultaneous time series of radiation, cloudiness and visibility. The first two are necessary to resolve the difference between clear and cloudy-sky signals in the radiation data, a method which in this paper has been called the determination of 'proxies'. Additional observations of visibility are necessary to understand the possible influence of aerosols on radiation.

There are a number of ways to improve and/or facilitate this work in the future:

1) The practice of observing different parameters simultaneously can be improved by a more optimum consideration of the impact of one parameter on another. For example aerosols and clouds impact radiation, but radiation is recorded as an hourly average, while clouds and visibility parameters are recorded as averages of smaller time intervals. Often these different recording and averaging intervals are based on WMO standards. Yet, they inhibit the analysis and interpretation of their physical links. It would be better if averaging times were standardized more uniformly or if the basic data underlying the averages become available.

2) The relative contribution to the all-sky radiation of cloud thickness remains unclear. Therefore, the potential impact of ACI-I and ACI-II cannot be unambiguously quantified. The best way to resolve this issue is by adding observations of clouds using a cloud radar and a cloud lidar. As clouds are largely transparent to radar probing cloud thickness and its long-term variations can thus be derived. Here, super-sites such as those of the Atmospheric Radiation Measurement program and CloudNet, or long-

term data from CloudSat could be of great assistance. Passive radiation data from satellites are less suitable as they only record radiation emanating from the top of clouds or from the layer just beneath cloud top.

3) The impact of changes in the single scattering albedo is unclear. This situation is best resolved by direct observations of the single scattering albedo including its wavelength dependence. However, this suggestion only works for future studies as observations of single scattering albedo have hardly been performed in the past. It may be that regional modelling of past aerosol composition and physical and optical properties may alleviate the historical lack of single scattering albedo data.

664   **Appendix A**

665

666   **A1.1 Averaging using real data**

667

668   Here we provide a full derivation of the analysis leading to Equations (1) and (3) in the main text. The essential

669   elements in this analysis are 1) A transition from 'real' data to 'proxy' data which constitutes a different way of

670   averaging yearly data, 2) Expressing the all-sky proxy radiation as a linear combination of clear-sky and cloud-

671   base proxy radiation, and 3) A perturbation analysis from which trends can be calculated.

672

673   We analyze the trends of time series of global radiation S_k where S is the yearly averaged global radiation and k

674   is the index of a year in the period 1966 – 2015. We write S_k as a function of two controlling variables:

675   fractional cloudiness c and cosine of solar zenith angle $\mu_0 = cos(\theta_0)$. Each of these two parameters varies

676   between 0 and 1 (i.e. when the sun is below the horizon the variable μ_0 is set to zero).

677

678   In the observations from meteorological stations the global radiation comes in discrete values, in our case as

679   hourly averages, 8760 or 8784 values in a year. Each of these hourly averages is thus assigned a specific value

680   of μ_0, namely the mid-point of the hour. The index i is the bin index of counting over μ_0. To build up the

681   probability space for μ_0 bins of μ_0 can be selected at the analyst's discretion (for example with width 0.05).

682

683   Observations of cloudiness are usually assigned in oktas. Okta values (0 – 8) are associated with specific

684   margins of fractional cloud coverage (see table 1 of Boers et al, 2010). We will designate the fractional

685   cloudiness associated with each okta value as c_j where j = 0 – 8. The yearly bivariate distribution function can

686   then be constructed as

687   $$p_k(\mu_{0i}, c_j) = \frac{N_{ijk}}{N_k}$$ (A1a)

688   where N_{ijk} is the number of observations in a single bin and

689   $$\sum_i \sum_j N_{ijk} = N_k \quad \text{and} \quad \sum_i \sum_j p_k(\mu_{0i}, c_j) = 1$$ (A1b,c)

690   Marginal distribution functions of Eq. (A1a) are

691   $$f_k(c_j) = \sum_i p_k(\mu_{0i}, c_j) = \frac{\sum_i N_{ijk}}{N_k} = \frac{N_{jk}}{N_k}$$ (A2)

692   where $f_k(c_j)$ is the fractional occurrence of cloud cover within a specific okta value, and

693   $$f(\mu_{0i}) = \sum_j p_k(\mu_{0i}, c_j) = \frac{\sum_j N_{ijk}}{N_k} = \frac{N_{ik}}{N_k}$$ (A3)

694   where $f(\mu_{0i})$ is the distribution of cosines of solar zenith angle. While the distribution $f(\mu_{0i})$ is invariant

695   with time as it is solely dependent on the latitude of the observations, $f_k(c_j)$ is varying with time due to yearly

696 and possible decadal trends. Yearly averaged fractional cloudiness c_k is found as the expected value of c of the

697 marginal distribution p_k

698 $$c_k = \sum_{j=1}^{8} c_j f_k(c_j) \qquad \text{(A4)}$$

699 The yearly averages S_k can be computed as the expected value of S, namely the double summation over all

700 values of c and μ_0 that jointly occur in a single year

701 $$S_k = \sum_i \sum_j S_k(\mu_{0i}, c_j) p_k(\mu_{0i}, c_j) \qquad \text{(A5)}$$

702 Here $S_k(\mu_{0i}, c_j)$ is the average value of S_k in the bin (i,j,k).

703 For each okta class we can derive the distribution of zenith angles as the conditionally sampled bivariate

704 distribution at the specific okta class c_j:

705 $$f_k(\mu_{oi}|c_j) = \frac{p_k(\mu_{0i}, c_j)}{f_k(c_j)} \qquad \text{(A6)}$$

706 We now obtain the yearly averaged global radiation in each okta class as the expected value of the hourly global

707 radiation data sampled conditionally with okta class:

708 $$S_{c_j,k} = \sum_i S_k(\mu_{0i}, c_j) f_k(\mu_{0i}|c_j) \qquad \text{(A7)}$$

709 Combining Eq. (A5), (A6) and (A7) yields

710 $$S_k = \sum_j f_k(c_j) S_{c_j,k} \qquad \text{(A8)}$$

711 Provided that there are adequate observations of cloudiness to select each observation of global radiation

712 according to the okta class in which it occurs, it is possible to calculate $S_{c_j,k}$ and hence S_k directly from the

713 observations.

714

715 The assumption we make at this point is that the hourly observation of radiation is a linear combination of a

716 clear-sky term and a cloud-base term, each weighted by their occurrence:

717

718 $$S_k(\mu_{0i}, c_j) = S_k(\mu_{0i}, c_0)(1 - c_j) + S_{k,cb}(\mu_{0i}, c_j) c_j \qquad \text{(A9)}$$

719

720 where $S_{k,cb}$ is the cloud-base radiation. Although Eq. (A9) is a customary approximation, it is almost certainly

721 incomplete as it neglects possible contributions to the flux from three-dimensional photon scattering between

722 clouds, in particular when cloud cover is broken. However, to our knowledge no useful correction to Eq. (A9)

723 has been published taking such scattering into account. To produce a yearly average this function is multiplied

724 by the conditional distribution f (from Equation A6) and summed over all observations occurring in the specific

725 okta class:

726

727 $$\sum_i S_k(\mu_{0i},c_j)f_k(\mu_{0i}|c_j) = \sum_i S_k(\mu_{0i},c_0)f_k(\mu_{0i}|c_j)(1-c_j) + \sum_i S_{k,cb}(\mu_{0i},c_j)f_k(\mu_{0i}|c_j)c_j$$

728 (A10)

729

730 We thus find that

731 $$S_{c_jk} = S_{c_0k}(1-c_j) + S_{cb,j,k}c_j + R_1 \qquad \text{(A11a)}$$

732 with

733 $$R_1 = \sum_i S_k(\mu_{0i},c_0)[f_k(\mu_{0i}|c_j) - f_k(\mu_{0i}|c_0)](1-c_j) \qquad \text{(A11b)}$$

734 And

735 $$S_{cb,j,k} = \sum_i S_{k,cb}(\mu_{0i},c_j)f_k(\mu_{0i}|c_j) \qquad \text{(A11c)}$$

736 In (A11c) all cloud base radiation in a single okta class is simply lumped together. We now calculate the total
737 radiation:

738

739 $$S_k = \sum_j S_{c_jk} \qquad \text{(A12a)}$$

740

741 With further manipulation we then find that

742

743
$$S_k = S_{c_0k}[1-\sum_{j=1}^{8} f_k(c_j)c_j] + \sum_{j=1}^{8} f_k(c_j)c_j S_{cb,c_{jk}} +$$
$$\sum_j f_k(c_j)\sum_i S_k(\mu_{0i},c_0)[f_k(\mu_{0i}|c_j) - f_k(\mu_{0i}|c_0)] \qquad \text{(A12b)}$$
$$= S_{c_0k}[1-c_k)] + c_k S_{cloud,k} + \sum_j \sum_i S_k(\mu_{0i},c_0)f_k(c_j)[f_k(\mu_{0i}|c_j) - f_k(\mu_{0i}|c_0)]$$

744 from which it follows that

745

746 $$S_k = S_{c_0k}[1-c_k] + c_k S_{cloud,k} + R_2 \qquad \text{(A13a)}$$

747 $$R_2 = \sum_j \sum_i S_k(\mu_{0i},c_0)f_k(c_j)[f_k(\mu_{0i}|c_j) - f_k(\mu_{0i}|c_0)] \qquad \text{(A13b)}$$

748

749 Here

750 $$S_{cloud,k} = \frac{\sum_{j=1}^{8} f_k(c_j)c_j S_{cb,c_jk}}{\sum_{j=1}^{8} f_k(c_j)c_j} \qquad \text{(A14)}$$

751

752 The rest terms R_1 and R_2 stem from the fact that the average value $S_{c_0 k}$ (A11a) is different for individual okta

753 classes as the summation is done over values of the cosine of solar zenith angle that are different for each okta

754 class. Nevertheless it is expected that both terms are small as the summations in R_1 and R_2 are done over small

755 terms that are positive as well as negative and thus will partly cancel. The parameter $S_{cloud,k}$ is the cloud-base

756 radiation weighted by cloud fraction.

757

758 **A1.2 Averaging using proxy data**

759 It has long been recognized that $S_{c_j k}$ has large year-to-year fluctuations because $p_k(\mu_{0i}, c_j)$ varies from

760 year-to-year. Extended periods of cloudiness of certain types that influence $p_k(\mu_{0i}, c_j)$ are associated with

761 synoptic systems that may occur randomly during the year. This means that trend analysis based on Eq. (A13)

762 will be subject to large uncertainties that can only be alleviated by collecting data over large areas so that

763 different synoptic systems are sampled at the same time (Liepert, 2002), or by averaging $S_{c_j k}$ over several years

764 and then performing trend analysis on the reduced and averaged data set (Liepert and Tegen, 2002)). Over a

765 relatively small region as the Netherlands Eq. (A13) is unsuitable to use. In fact Ruckstuhl et al (2010)

766 demonstrated that the use of the radiation data in its pure form would lead to wrong interpretations of trends. To

767 reduce the uncertainty in estimates of $S_{c_j k}$, in particular when estimating the global radiation under cloudless

768 skies $S_{c_0 k}$ some investigators have resorted to fitting an 'umbrella' function of clear-sky radiation over all

769 observations within one year (Long et al, 2009; Ruckstuhl et al, 2010) based for example on discrimination of

770 clear skies by analysis of direct and diffuse radiation. In our formulation the approach of fitting an umbrella

771 function is equivalent to a procedure whereby $S_k(\mu_{0i}|c_0)$ is fitted by a function $G_{c_0 k}(\mu_{0i})$. When we

772 proceed in this way, the parameter $S_{p,c_0 k}$ which is a proxy for $S_{c_0 k}$ is calculated as

773 $$S_{p,c_0 k} = \sum_i G_{c_0 k}(\mu_{0i}) f(\mu_{0i}) \qquad (A15)$$

774 There are strong theoretical arguments to suggest that $G_{c_0 k}(\mu_{0i})$ is a monotonically increasing function of μ_{0ik}

775 given a specific value of c_j. The use of the marginal distribution $f(\mu_{0i})$ in the summation assures that the

776 entire distribution of cosines of solar zenith angles representative for the location at hand is used in the

777 calculation rather than conditional distribution $f_k(\mu_{0i}|c_0)$ which is highly variable from year-to-year and for

778 which only a summation over a limited set of observations can be used.

779

780 In this paper the approach will be to generalize Eq. (A15) to all nine okta values as

781 $$S_{p,c_j k} = \sum_i G_{c_j k}(\mu_{0i}) f(\mu_{0i}) \qquad (A16).$$

782 In other words we will calculate functions of the type $G_{c_j k}(\mu_{0i})$ for each okta value using the observations at

783 hand.

784

785   The notion that the functions $G_{c_jk}(\mu_{0i})$ are monotonic increasing with μ_{01} comes from Beer's Law stating that

786   for a single wavelength only the optical thickness of the atmosphere and μ_{0i} itself are parameters controlling the

787   change in downwelling radiation with μ_{0i}

788     $$S_s = \mu_0 S_e \exp(-\tau / \mu_0) \qquad\qquad\qquad (A17)$$

789   Here S_s is the downwelling radiation at the surface, S_e is the extraterrestrial radiation, and τ is the optical

790   thickness of the atmosphere.

791

792   Even though the global radiation is a wavelength-integrated quantity, the scattering through the atmosphere

793   consisting of water droplets, ice crystals and aerosols at high relative humidity can in first order be assumed to

794   be conservative. Therefore, it is reasonable to assume that $G_{c_jk}(\mu_{0i})$ has a functional form resembling Eq.

795   (A17). When regressed through data taken over an entire year the fitted line has a parameter akin to the yearly

796   averaged optical thickness of the atmosphere as its sole controlling variable.

797

798   Consequently, we will adopt the function

799     $$G(\mu_0) = \mu_0 A \exp(-B / \mu_0) \qquad\qquad\qquad (A18)$$

800   where B is a parameter depending on μ_0 according to

801     $$B(\mu_0) = \alpha \mu_0{}^\beta \qquad\qquad\qquad\qquad (A19)$$

802   The parameters α and β are constants determined by fitting the data. The method expressed in Eq (A18) is

803   equivalent to the Langley method of obtained optical thickness with the only difference the weak dependence of

804   B on sun angle. Such dependence is necessary to include because the diffuse radiation arriving at the surface is

805   weakly dependent upon μ_0,

806

807   Following the procedure outlined for the real data exactly but including the subscript p to indicate 'proxy' and

808   changing the conditional distributions (A6) with the marginal distribution (A3) we can finally write for the

809   proxy global radiation

810     $$S_{pk} = S_{p,c_0k}(1 - c_k) + c_k S_{p,cloud,k} \qquad\qquad (A20)$$

811   where $S_{p,cloud,k}$ is obtained from an equation identical to Eq. (A9) with $S_{cb,k}$ replaced by $S_{p,cb,k}$. Note

812   however that the rest terms R_1 and R_2 have vanished in the proxy formulation. The reason is that the conditional

813   distributions have been replaced by the marginal distribution of cosine of solar zenith angles, which is

814   independent of cloud cover fraction and time. Therefore the marginal distributions in the rest term are all

815   identical and thus will cancel exactly. Equation (A20) is represented in the main text as Eq. (1).

816

817   Eq (A19) expresses the dependence of atmospheric optical thickness on μ_0. Regression fits using Eq. (A19)

818   carries uncertainties into the parameter B and through Eq. (A18) into parameter G and into Eq. (A20). For clear-

819   sky the scatter is small but for skies under (partly) cloudy skies the scatter is larger. The standard 1-sigma

820 uncertainty associated with the clear sky proxy computed in Eq. (A20) is 2-3%, increasing to 8-9 % for high
821 okta values.

822

823 The year-to-year determination of proxies in Eq. (A20) is used in this paper as it will yield more stable results
824 than the determination of 'true' averages. The approach will avoid all seasonal elements and yearly variations
825 that are inherent in the distribution $f_k(\mu_{0i}|c_j)$ due to the yearly variable numbers of μ_{0i} values necessary to
826 compute the conditionally sampled data. Therefore, the computed trends of proxies will reflect the yearly
827 changing transmission through the atmosphere, which is the purpose of this study.

828

829 Note finally that $S_k \neq S_{pk}$ as the proxy analysis is based on an evaluation of proxy fluxes, not of the 'real'
830 fluxes. In the analysis to be performed, however, differences between them turned out to be less than 5%.
831

832 **A1.3 Analysis of trend**

833 Once a time series of proxy radiation values is obtained it is possible to compute trends. As explained in the
834 previous section trends in the observed time series of clear-sky and cloudy sky radiation are not very useful due
835 to the year-to-year variability. However, trends in the proxy radiation time series do not suffer from such noise
836 and thus can yield meaningful results. A single equation will be derived for the trend in all-sky (proxy) radiation
837 from which it emerges that such trend is the result of three components: a) a trend in fractional cloudiness, b) a
838 trend in clear sky radiation and c) a trend in radiation at cloud-base.

839

840 To derive trends from the yearly averages (proxy) data we write:

841
$$c_k = \overline{c} + c'_k, \quad S_{p,c_0,k} = \overline{S_{p,c_0}} + S'_{p,c_0,k}, \quad S_p(y_k) = \overline{S_p} + S'_p(y_k), \quad S_{p,cloud,k} = \overline{S_{p,cloud}} + S'_{p,cloud,k}$$

842 (A21)

843

844 Here the bar represents an average over 5 decades of the yearly averages, and the primed variables are the yearly
845 deviations from the averages over the five decades under analysis. Inserting into Eq. (A20) yields

846

847
$$S_{pk} = \overline{S_p} + S'_{pk} = (1 - \overline{c} - c'_k)(\overline{S_{p,c_0}} + S'_{p,c_0k}) + (\overline{c} + c'_k)(\overline{S_{p,cloud}} + S'_{p,cloud,k}) \qquad (A22)$$

848 Defining $\quad \overline{S_p} = (1-\overline{c})\overline{S_{p,c_0}} + \overline{c}\,\overline{S_{p,cloud}} \quad$ and collecting terms yields

849
$$S'_k = c'_k(\overline{S_{p,cloud}} - \overline{S_{p,c_0}}) + (1-\overline{c})S'_{p,c_0k} + \overline{c}S'_{p,cloud,k} + c'_k(S'_{cloud,k} - S'_{p,c_0k}) \qquad (A23)$$

850 Eq (A23) can be used for trend analysis and is represented in the main text as Eq. (3).

851 The implications of this expression are quite important. Eq. (A23) demonstrates that the trend in all-sky
852 radiation is not a simple summation of trends in clear-sky and cloudy-sky trends, which would perhaps be an
853 intuitive notion when seeking to explain the observed trend in all sky radiation. Eq. (A23) demonstrates that a)
854 the trends in clear-sky and cloud-base radiation need to be weighted by their fractional occurrence in the

855 atmosphere, and that b) there is a third term constituting the trend in fractional cloudiness scaled by the

856 difference in average cloud-base and clear-sky radiation. Furthermore, the additional fourth term, which is

857 shown to be negligible in the current analysis, may not always be small when there are significant cross

858 correlations between the perturbations.

859

Data availability

The data used in this paper can be downloaded from the KNMI website:

http://www.knmi.nl/nederland-nu/klimatologie/uurgegevens

Acknowledgments

We acknowledge the use of EUMETSAT's CMSAF cloud climatology data sets. We much appreciated discussions with Jan Fokke Meirink who made us aware of this data set and who instructed us on its use in this analysis. We also appreciated discussion with Wiel Wauben about the break analysis.

869   **Tables**

870

871   **Table 1**: **Details of the stations and the introduction data of the radiometers.**

Station	WMO nr.	LAT (N)	LON (E)	ALT (m)	Introduction date
De Kooy	06235	52.924	4.785	0.5	24 September 1964
De Bilt	06260	52.101	5.177	2.0	10 May 1957
Eelde	06280	53.125	6.586	3.5	2 October 1964
Vlissingen	06310	51.442	3.596	8.0	10 April 1962
Maastricht	06380	50.910	5.768	114.0	5 March 1963

872
873

874 **Table 2. Summary of trend analysis. Except for the fractional cloudiness, all parameters have W m^{-2} /**

875 **decade as a unit. Whether or not the indicated trend is significant is indicated by the star in the column**

876 **'uncertainty'.**

Type	Period	Trend	Uncertainty
Fractional cloudiness	1966-2015	0.0097	0.0062*
	1966-1984	-0.0055	0.0344
	1984-2015	0.0205	0.0117*
All-sky radiation	1966-2015	1.81	1.07*
	1966-1984	-1.40	4.19
	1984-2015	3.30	1.55*
All-sky proxy radiation	1966- 2015	1.89	0.78*
	1966- 1984	0.39	3.86
	1984- 2015	2.30	1.68*
Clear-sky proxy radiation	1966-2015	2.78	0.50*
	1966-1984	1.22	2.14
	1984-2015	3.46	1.35*
Cloud-base proxy radiation	1966-2015	3.43	1.17*
	1966-1984	-0.77	2.01
	1984-2015	4.94	2.30*
Fractional cloudiness term of Equation (3)	1966-2015	-1.06	0.67*
	1966-1984	0.43	3.30
	1984-2015	-2.22	1.19*
Clear-sky proxy term of Equation (3)	1966-2015	0.88	0.16*
	1966-1984	0.39	0.68
	1984-2015	1.09	0.43*
Cloud-base proxy term of Equation (3)	1966-2015	2.35	0.80*
	1966-1984	-0.53	1.38
	1984-2015	3.37	1.57*

877

878 **Figures**
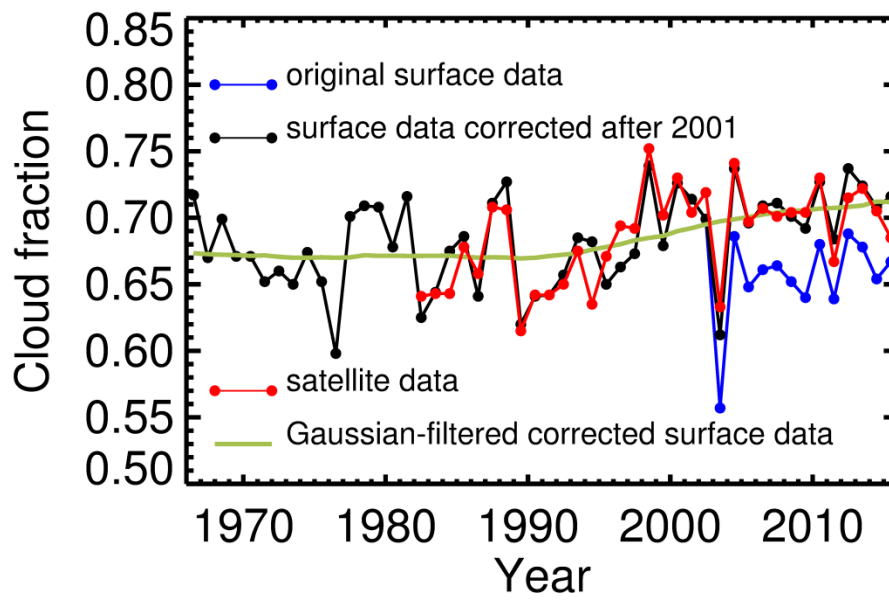
879

880 **Figure 1**. **Surface-based cloud fraction estimates versus satellite-based estimates.**

881
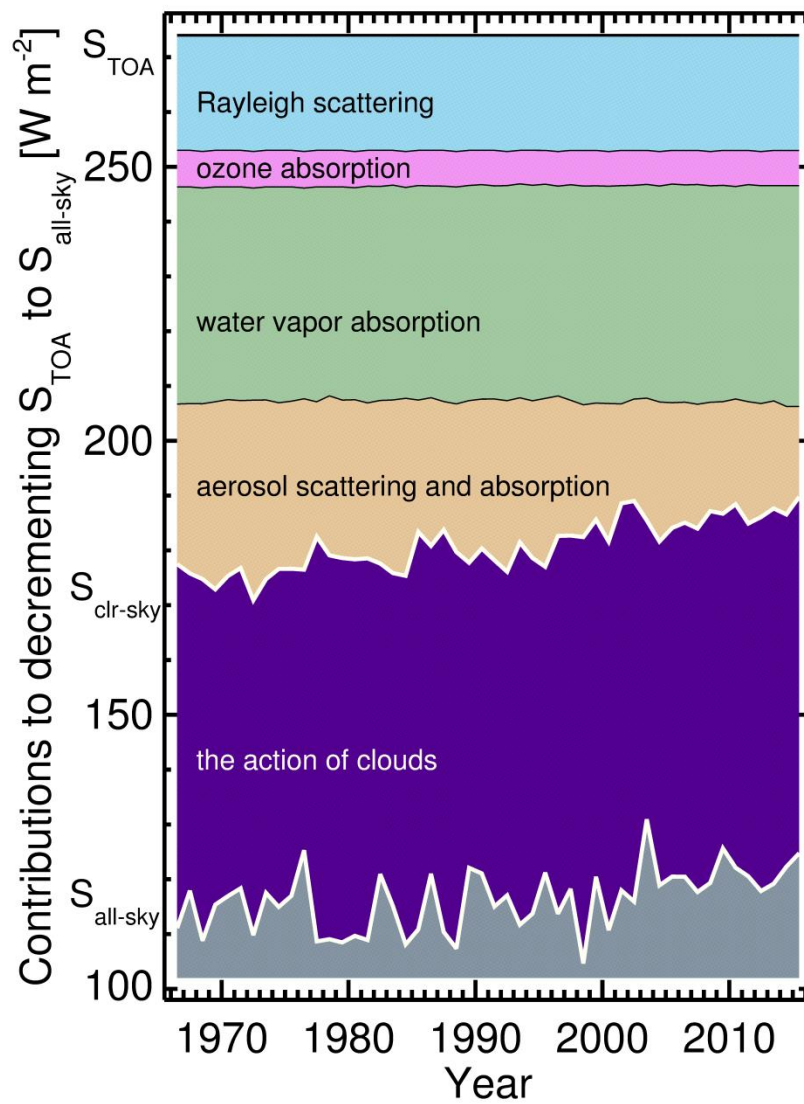
Figure 2. Impact on all-sky flux due to Rayleigh scattering, ozone absorption, water vapor absorption, aerosol scattering and absorption and the action of clouds.
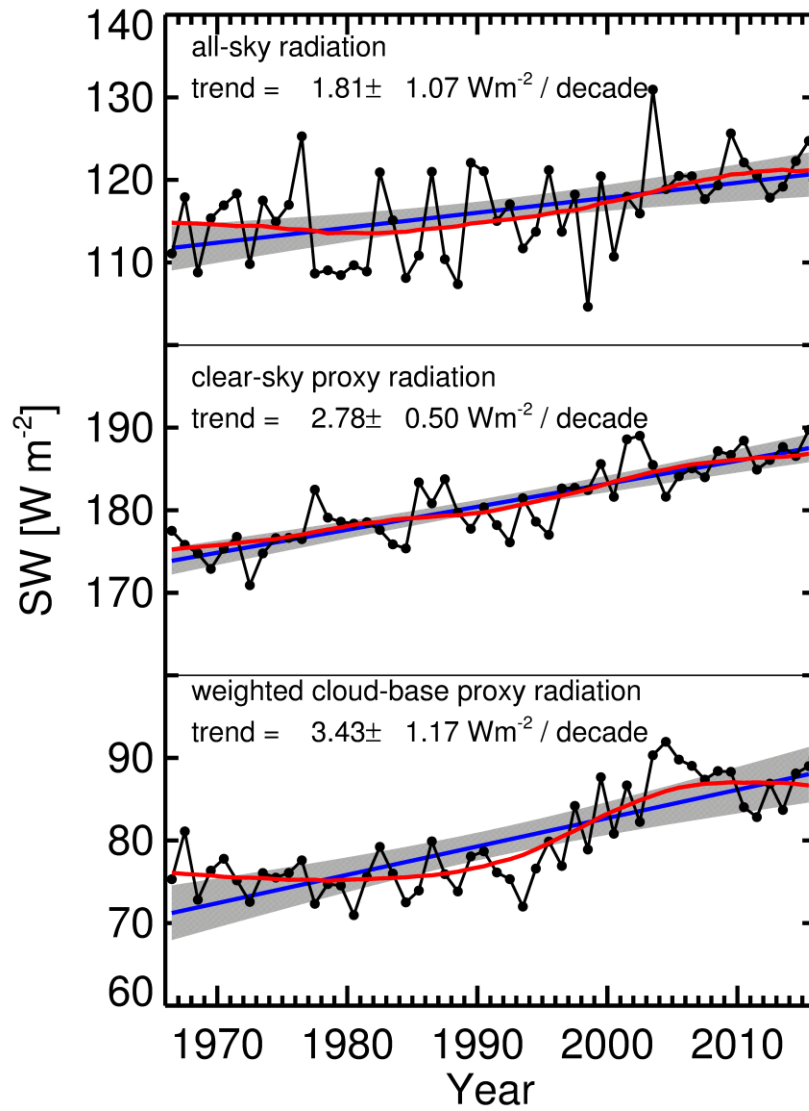
886

887 **Figure 3**. **All-sky, clear-sky proxy and cloud-base proxy radiation as a function of time. Blue lines are the**

888 **regression fits with the grey area as the uncertainty around the fit. The red lines are 21-point Gaussian**

889 **filter smoothers.**

890

891
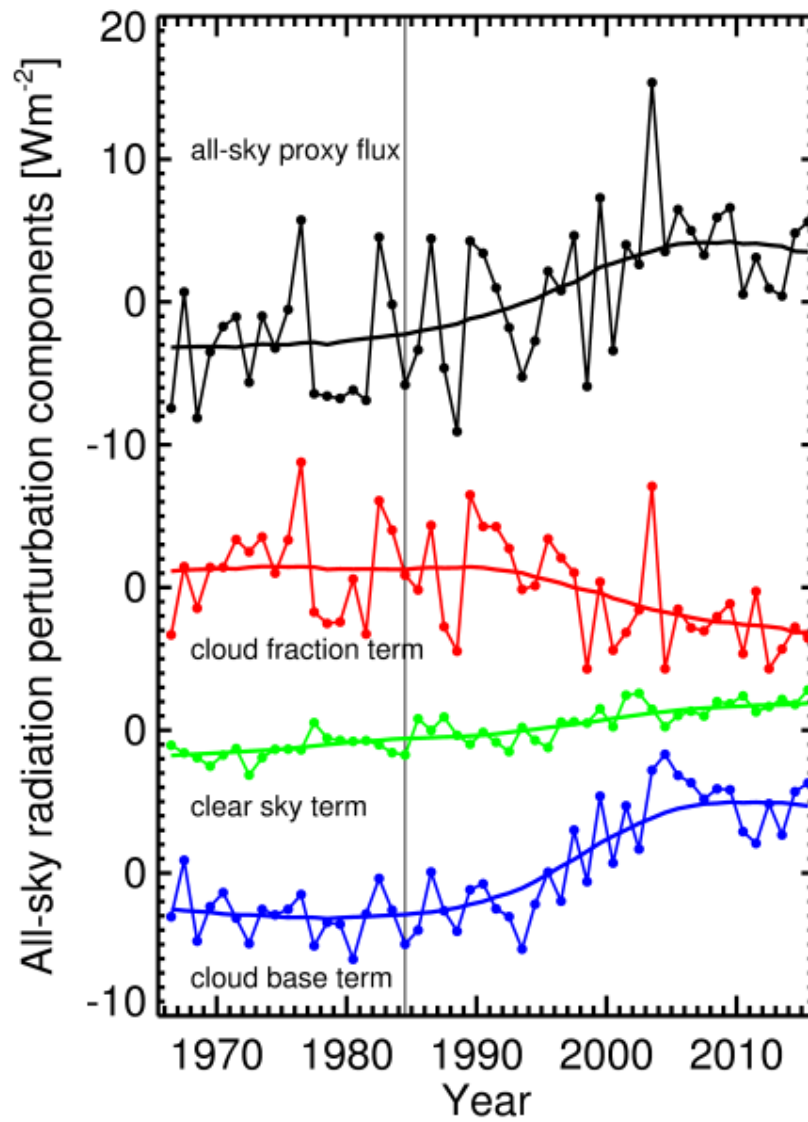
Figure 4. All-sky radiation perturbation components. Terms are indicated in the graph. 21-point Gaussian filter smoothers are drawn through the curves.

894

895
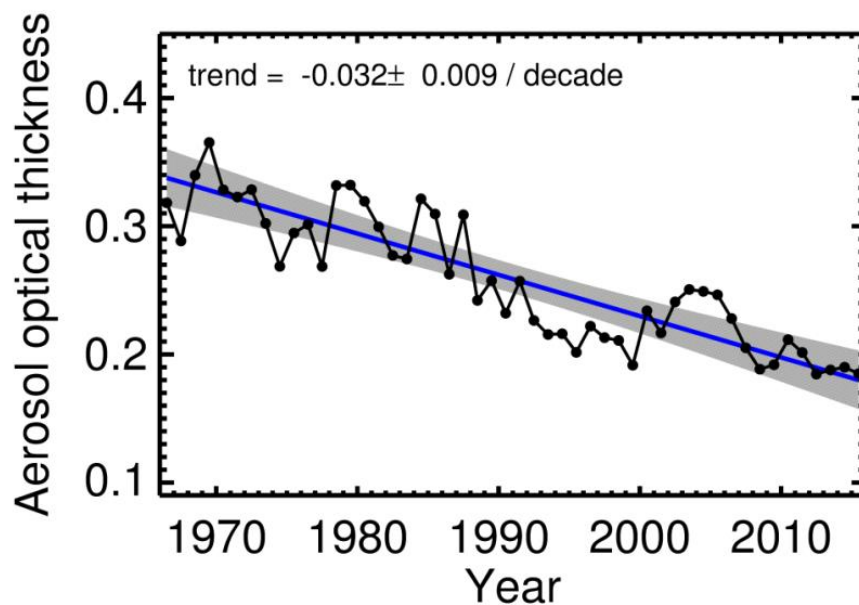
896   **Figure 5**. **Aerosol optical thickness derived from visibility observations.**

897

898
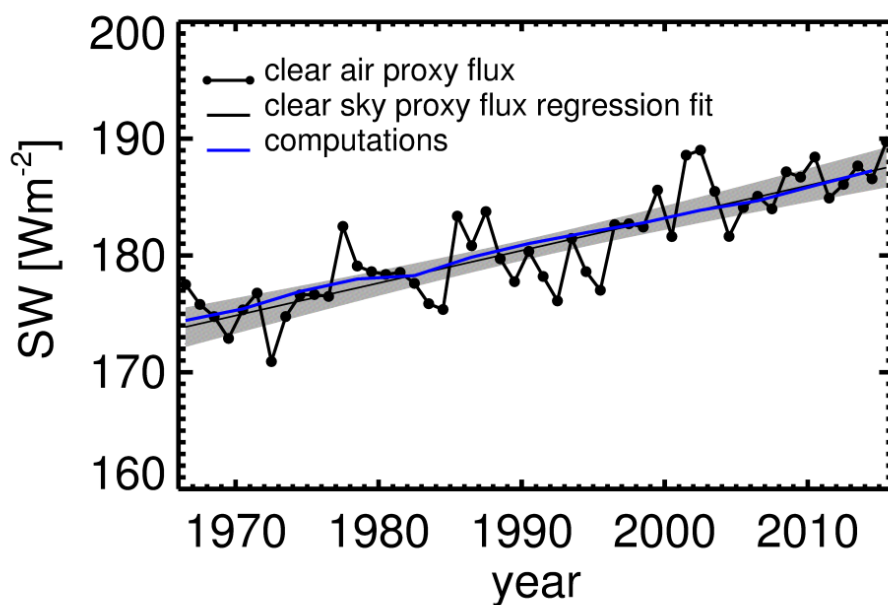
899   **Figure 6**. **Clear-sky radiation observations matched by radiative transfer computations.**

900
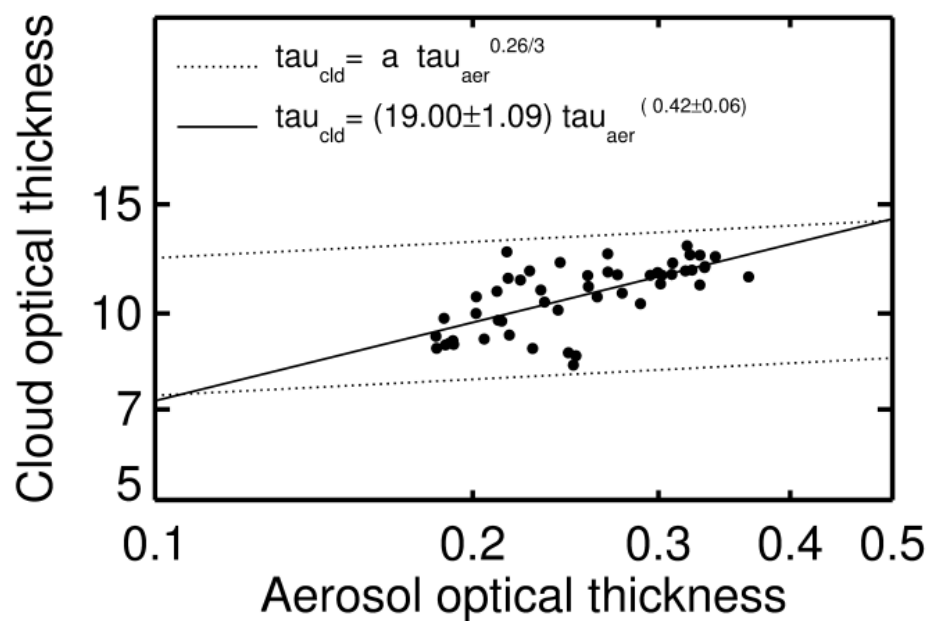
901

902 **Figure 7**. **Cloud optical thickness as a function of aerosol optical thickness. The broken lines are the**
903 **suggested dependencies of the two optical thicknesses assuming that ACI-I is valid. The solid line is the**
904 **actual fit through the data.**

905

906 **References**

907 Albrecht, B. A., Aerosols, cloud microphysics and fractional cloudiness, Science, 245, 1227 – 1230, 1989.
908

909 Alexanderson H., A homogeneity test applied to precipitation data, J. of Clim., 6, 661-675, 1986.
910

911 Augustine, J. A. and E.G. Dutton, Variability of the surface radiation budget over the United States from 1996
912 through 2011 from high-quality measurements, J. Geophys. Res., 118, doi:10.1029/2012JD018551.

913 Boers, R and R. M. Mitchell, Absorption feedback in stratocumulus cloud: Influence on cloud top albedo,
914 Tellus, 46A, 229 – 241, 1994.
915

916 Boers, R., M. J. de Haij, W. M. F. Wauben, H. K. Baltink, L. H. van Ulft, M. Savenije, and C. N. Long,
917 Optimized fractional cloudiness determination from five ground-based remote sensing techniques, J. Geophys.
918 Res., 115, D24116, doi:10.1029/2010JD014661, 2010.
919

920 Boers, R., M. van Weele, E. van Meijgaard, M. Savenije, A.P. Siebesma, F. Bosveld and P. Stammes,
921 Observations and projections of visibility and aerosol optical thickness (1956–2100) in the Netherlands: Impacts
922 of time-varying aerosol composition and hygroscopicity, Environ. Res. Lett. ,10, 015003, doi:10.1088/1748-
923 9326/10/1/015003, 2015.
924

925 Chiacchio, M., and M. Wild, Influence of NAO and clouds on long-term seasonal variations of surface solar
926 radiation in Europe, J. Geophys. Res., 115, D00D22, doi:10.1029/2009JD012182, 2010.

927

928 Dee, D. et al., The ERA-Interim reanalysis: configuration and performance of the data assimilation system.
929 Quart.. Journal Roy. Meteor. Soc., **137**, 553 – 597, 2010.
930

931 Eltermann, L, Relationships between vertical attenuation and surface meteorological range, Appl. Optics., 9,
932 1804–1810., doi:10.1364/ AO.9.001804, 1970.
933

934 Gan, C.-M., J. Pleim, R. Mathur, C. Hogrefe, C. N. Long, J. Xing, S. Roselle, and C. Wei, Assessment of the
935 effect of air pollution controls on trends in shortwave radiation over the United States from 1995 through 2010
936 from multiple observation networks. Atmos. Chem. Phys., 14, 1701–1715, 2014, www.atmos-chem-
937 phys.net/14/1701/2014/doi:10.5194/acp-14-1701-2014, 2014.
938

939 Gultepe, I and G. A. Isaac, The relationship between cloud droplet and aerosol number concentration for
940 climate models. Int. J. Climat. 16, 941 – 946, 1995.
941

942 IPCC, Climate Change 2013: The Physical Science Basis. Contribution of Working Group I to the Fifth
943 Assessment Report of the Intergovernmental Panel on Climate Change [Stocker, T.F., D. Qin, G.-K. Plattner, M.
944 Tignor, S.K. Allen, J. Boschung, A. Nauels, Y. Xia, V. Bex and P.M. Midgley (eds.)]. Cambridge University

945 Press, Cambridge, United Kingdom and New York, NY, USA, 1535 pp, doi:10.1017/CBO9781107415324,
946 2013.

947

948 Jones, A, D. L. Roberts and A. Slingo, A climate model study of indirect radiative forcing by anthropogenic
949 sulphate aerosols. Nature, 370, 450 − 453, 1994.

950

951 Karlsson, K.-G., Anttila, K., Trentmann, J., Stengel, M., Meirink, J. F., Devasthale, A., Hanschmann, T., Kothe,
952 S., Jääskeläinen, E., Sedlar, J., Benas, N., van Zadelhoff, G.-J., Schlundt, C., Stein, D., Finkensieper, S.,
953 Håkansson, N., and Hollmann, R., CLARA-A2: The second edition of the CM SAF cloud and radiation data
954 record from 34 years of global AVHRR data, Atmos. Chem. Phys. Discuss., doi:10.5194/acp-2016-935, revised
955 manuscript accepted for publication in ACP..

956

957 Kendall, M.G., Rank Correlation Methods, 4th edition, Charles Griffin, London, 1975.

958

959 Kriebel, K. T., On the determination of the atmospheric optical depth by measurements of the meteorological
960 range, Beitr. Phys. Atmos., 51, 330, 1978.

961

962 Li, H., J. Sheffield, and E. F. Wood, Bias correction of monthly precipitation and temperature fields from
963 Intergovernmental Panel on Climate Change AR4 models using equidistant quantile matching, J. Geophys. Res.,
964 115, D10101, doi:10.1029/2009JD012882, 2010.

965

966 Liepert, B. G., Observed reductions of surface solar radiation at sites in the United States and worldwide from
967 1961 to 1990, Geophys. Res. Lett., 29, 10, 1421, 10.1029/2002GL014910, 2002.

968

969 Liepert. B. G., Recent changes in solar radiation under cloudy conditions in Germany. Intern. J. climatology 17,
970 1581 − 1593, 1997.

971

972 Liepert, B and I. Tegen, Multidecadal solar radiation trends in the United States and Germany and direct
973 tropospheric aerosol forcing. J. Geophys. Res., 107, D12, 4153, 10.1029/2001JD000760, 2002.

974 Liepert, B. and G. Kukla, Decline in solar radiation with increased horizontal visibility in Germany between
975 1964 and 1990. Journal of Climate, 10, 2391 − 2401, 1997.

976

977 Long , C. N., and T. P. Ackerman, Identification of clear skies from broadband pyranometer measurements and
978 calculation of downwelling shortwave cloud effects, J. Geophys. Res., 105, D12, 15,609-15, 626, 2000.

979

980 Long, C. N., E. G. Dutton, J. A. Augustine, W. Wiscombe, M. Wild, S. A. McFarlane, and C. J. Flynn,
981 Significant decadal brightening of downwelling shortwave in the continental United States, J. Geophys. Res.,
982 114, D00D06, doi:10.1029/2008JD011263, 2009.

983

Manara, V, M. Brunetti, A. Celozzi, M. Maugeri, A. Sanchez-Lorenzo, and M. Wild, Detection of dimming/brightening in Italy from homogenized all-sky and clear-sky surface solar radiation records and underlying causes (1959–2013), Atmos. Chem. Phys., 16, 11145–11161, doi:10.5194/acp-16-11145-2016, 2016.

Mateos, D., A. Sanchez-Lorenzo, M. Antón,V. E.Cachorro, J. Calbó, M. J. Costa, B. Torres, and M. Wild, Quantifying the respective roles of aerosols and clouds in the strong brightening since the early 2000s over the Iberian Peninsula, J. Geophys. Res. , 119, 10,382–10,393, doi:10.1002/2014JD022076, 2014.

Norris, J. R., Multidecadal changes in near-global cloud cover and estimated cloud cover radiative forcing, J. Geophys. Res., 110, D08206, doi:10.1029/2004JD005600, 2005.

Norris, J. R., and M. Wild, Trends in aerosol radiative effects over Europe inferred from observed cloud cover, solar ''dimming,'' and solar ''brightening'', J. Geophys. Res., 112, D08214, doi:10.1029/2006JD007794, 2007.

Ohvril, H., et al., Global dimming and brightening versus atmospheric column transparency, Europe, 1906–2007, J. Geophys. Res., 114, D00D12, doi:10.1029/2008JD010644, 2009.

Parding, K,, J. A. Olseth , K. F. Dagestadt and B. G. Liepert, Decadal variability of clouds, solar radiation and temperature at a high-latitude coastal site in Norway, Tellus B 66, 25897, 2014.

Peterson, J. T., and C. J. Fee, Visibility-atmospheric turbidity dependence at Raleigh, North Carolina, Atmos. Environ, 15(12), 2561-2563, 1981.

Philipona, R.,K. Behrens, and C. Ruckstuhl, How declining aerosols and rising greenhouse gases forced rapid warming in Europe since the 1980s, Geophys. Res. Lett., 36, L02806, doi:10.1029/2008GL036350, 2009.

Romanou, A., B. Liepert, G. A. Schmidt, W. B. Rossow, R. A. Ruedy, and Y. Zhang, 20th century changes in surface solar irradiance in simulations and observations, Geophys. Research Lett. 34, L057113, doi: 10.1029/2006GL028356, 2007.

Ruckstuhl, C., and J. R. Norris, How do aerosol histories affect solar ''dimming'' and ''brightening'' over Europe?: IPCC-AR4 models versus observations, J. Geophys. Res., 114, D00D04, doi:10.1029/2008JD011066, 2009.

Ruckstuhl, C., J. R. Norris, and R. Philipona, Is there evidence for an aerosol indirect effect during the recent aerosol optical depth decline in Europe?, J. Geophys. Res., 115, D04204, doi:10.1029/2009JD012867, 2010.

Ruckshuhl, C. and R. Philipona, Detection of cloud-free skies based on sunshine duration and on the variation of global solar irradiance, Meteor. Zeitschrift, 17, No. 2, 181-186, 2008.

1024

1025 Ruckstuhl, C., R. Philipona, K. Behrens, M. Collaud Coen,B. Durr, A. Heimo, C. Matzler, S. Nyeki, A.
1026 Ohmura, L. Vuilleumier, M. Weller, C. Wehrli, and A. Zelenka, Aerosol and cloud effects on solar brightening
1027 and the recent rapid warming, Geophys. Res. Lett, 35, L12708, doi:10.1029/2008GL034228, 2008.

1028

1029 Russak, V., Changes in solar radiation and their influence on temperature trend in Estonia (1955–2007), J.
1030 Geophys.Res., 114, D00D01, doi:10.1029/2008JD010613, 2009.

1031

1032 Sanchez-Lorenzo, A., M. Wild, M. Brunetti, J. A. Guijarro, M. Z. Hakuba, J. Calbó, S. Mystakidis, and B.
1033 Bartok, Reassessment and update of long-term trends in downward surface shortwave radiation over Europe
1034 (1939–2012), J. Geophys. Res. Atmos., 120, 9555–9569, doi:10.1002/2015JD023321, 2015.

1035

1036 Stjern, C. W., J.E. Kristjansson and A. W. Hansen, Global dimming and global brightening – an analysis of
1037 surface radiation and cloud cover data in northern Europe. Int. J. Climatol. 29: 643–653, 2009.

1038

1039 Turnock, S.T., D. V. Spracklen, K. S. Carslaw, G. W. Mann, M. T. Woodhouse, P. M. Forster, J. Haywood, C.
1040 E. Johnson, M. Dalvi, N. Bellouin, and A. Sanchez-Lorenzo, Modelled and observed changes in aerosols and
1041 surface solar radiation over Europe between 1960 and 2009 Atmos. Chem. Phys., 15, 9477–9500, www.atmos-
1042 chem-phys.net/15/9477/2015/ doi:10.5194/acp-15-9477-2015, 2015.

1043

1044 Twomey, S., The influence of pollution on the shortwave albedo of clouds, J. Atmos. Sci., 34, 1149 – 1152,
1045 DOI: http://dx.doi.org/10.1175/1520-0469(1977)034, 1977.

1046

1047 Wang, K. C., R. E. Dickinson, and S. L. Liang, Clear-sky visibility has decrease over land globally from 1973 to
1048 2007, Science, 323, 1468–1470, doi:10.1126/science.1167549, 2009.

1049

1050 Wild, M., Global dimming and brightening: A review, J. Geophys. Res., 114, D00D16,
1051 doi:10.1029/2008JD011470, 2009.

1052

1053 Wild, M., H. Gilgen, A. Roesch, A.Ohmura, C. N. Long, E. G. Dutton, B. Forgan, A. Kallis, V. Russak, A.
1054 Tsvetkov, From Dimming to Brightening: Decadal Changes in Solar Radiation at Earth's surface. Science, 308,
1055 , 847, Doi: 10.1126/science.1103215, 2005.

1056

1057 Wild, M., Introduction to special section on Global Dimming and Brightening, J. Geophys. Res., 115, D00D00,
1058 doi:10.1029/2009JD012841, 2010.

1059

1060 World Meteorological Organization (WMO), WMO guide to meteorological instruments and methods of
1061 observation, 7th ed., WMO-No. 8, Geneva, Switzerland, 2008.

1062

1063   Wu, J., J. Luo, L. Zhang, L. Xia, D. Zhao, and J. Tang, Improvement of aerosol optical depth retrieval using

1064   visibility data in China during the past 50 years, J. Geophys. Res., 119, 13,370–13,387,

1065   doi:10.1002/2014JD021550, 2014.

1066